ACS SENSORS

Article

Cite This: ACS Sens. 2018, 3, 222–229

pubs.acs.org/acssensors

Integrating Metal-Enhanced Fluorescence and Surface Acoustic Waves for Sensitive and Rapid Quantification of Cancer Biomarkers from Real Matrices

Jun Liu, Shuangming Li, and Venkat R. Bhethanabotla*

Department of Chemical & Biomolecular Engineering, University of South Florida, Tampa, Florida 33620-5350, United States

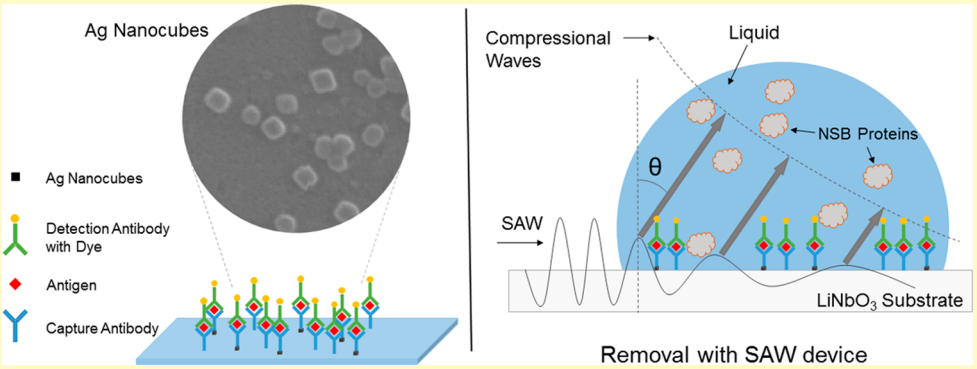

ABSTRACT: Metal-enhanced fluorescence (MEF) is utilized to lower the detection limit of carcinoembryonic antigen (CEA), a prognostic biomarker for colorectal cancer among others, in immunofluorescence assays. In addition, Rayleigh surface acoustic waves (SAWs) were utilized to remove nonspecifically bound proteins, improve mixing, and reduce incubation times. Fluorescence intensity was plasmonically enhanced by incubating silver nanocubes (AgNCs) of 50 nm edge-length on a SAW device. This increased sensor sensitivity by a factor of 6 and lowered the limit of detection to below 1 ng/mL in fluorescence detection of the antigen. Surface density of the AgNCs was optimized to produce the largest MEF, which increased the signal intensity by an order of magnitude. Acoustic streaming induced by Rayleigh SAWs was found to decrease antibody/antigen incubation times to 1/6th of the values without such micromixing, and to increase the fluorescence signal strength. Overall, the demonstrated results allow for construction of a sensor capable of detecting CEA rapidly in clinically relevant concentrations. Variables relevant for optimizing this sensor performance were identified, which will enable even better performance in immunofluorescence assays.

KEYWORDS: *silver nanocubes, metal-enhanced fluorescence, CEA, surface acoustic wave, limit of detection*

Cancer has become one of the most threatening diseases to human health worldwide and has caused 8.2 million deaths in 2014.[1] Tumor markers have been identified to help diagnose cancers and monitor disease progression by their concentration levels in body fluids. Gold and Freedman[2] first introduced carcinoembryonic antigen (CEA) as the tumor associated antigen in 1965. Although the clinical value of CEA has not been clarified completely, it has been accepted widely as the marker of gastrointestinal cancers over the past 40 years. According to many reports, 2.5 ng/mL of CEA is accepted to be the critical value to estimate the possibility of having gastrointestinal cancers or malignancy.[3−5]

Immunoassays are mostly developed for detecting proteins at the present time.[6] Among the various methods, immunofluorescence (IF) assays are widely used because both location and quantitative information on proteins can be gathered by visualizing specific antigen/antibody interactions with fluorophores. However, there are some limitations to this technique, with the primary ones being the high limit of detection (LOD) compared to other detection techniques, and a low working efficiency. Typically, the poor LOD of IF assays hinders applications for concentrations lower than 1 μg/mL.[6] Additionally, the whole assay process has poor efficiency, sometimes taking several hours to days to finish the detection.

To detect CEA at the clinically significant level, metal-enhanced fluorescence (MEF) was utilized in this work to lower the LOD of the IF assays to subnanogram/milliliter levels using silver nanocubes (AgNCs). MEF as a phenomenon is known for a few years, and has drawn attention in fluorescence applications. The ability of several metal particles to enhance the intensity in IF, especially gold and silver nanoparticles, has been reported.[7−12] Aslan et al.[13] reviewed the development of MEF in detection applications from DNA hybridization to labeled antigen/antibody. A 3- to 5-time enhancement was observed with a SiO_2-coated silver colloid sensing platform in detecting Cy3-labeled streptavidin.[14] The cardiac marker

Received: November 24, 2017
Accepted: December 29, 2017
Published: December 29, 2017

DOI: 10.1021/acssensors.7b00876
ACS Sens. 2018, 3, 222–229

myoglobin gained a 10- to 15-fold enhancement for the fluorophore-labeled antibody on silver island films.[13] MEF is a powerful tool in biotechnology for detecting proteins or DNA in cells *in vitro*.

Several factors like distance between metal particles and fluorophores, size and shape of the metal nanoparticles, the type of fluorophores, composition of the nanoparticle, and the compatibility of the proteins and DNA can affect enhancement significantly.[7,11,15,16] Generally, the interactions between excited states of the fluorophores and the induced surface plasmons of metal nanoparticles result in increased quantum yield and increased lifetime of fluorophores. While the former causes enhancement of intensity, the latter improves photostability of the fluorophores. In this work, AgNCs were found to effectively increase the signal by around 4.6 times and decrease photobleaching. With the enhancement provided by MEF, the detection limit was lowered down to less than a nanogram/milliliter levels. A comparison with several methods reported in the literature for detecting CEA with this work is presented in Table 1.

Table 1. Comparison of Different Methods for Detecting CEA

	method	LOD	cost
Huber et al.[17]	ELISA kits	>10 ng/mL	Medium
Tang et al.[18]	Electrical Impedance Spectroscopy (EIS)	~0.5 ng/mL	High
Chon et al.[19]	SERS Immunoassay	>3 ng/mL	Medium
This work	MEF-SAW	<1 ng/mL	Low

To overcome the low attachment efficiency in IF assays, a surface acoustic wave (SAW) device was utilized to increase the binding percentage between targets and shorten the incubation time required substantially. The SAW devices were designed to propagate Rayleigh waves along the surface of piezoelectric lithium niobate ($LiNbO_3$) by patterning of suitable interdigital transducers (IDTs) photolithographically. Acoustic streaming induced by the Rayleigh waves has been shown in our previous work to cause mixing of the fluid layer adjacent to the surface. Paxton et al.[20] demonstrated the effect of increased mixing on the ion exchange rates for plutonium in small volume samples. Toegl et al.[21] presented SAW streaming to overcome diffusion limitations to improve signal-to-noise ratio by a factor of 6 in their hybridization experiment with DNA, in addition to reducing the hybridization duration and improving homogeneity. The acoustic wave speeds up the movement of proteins, which increases the chance of their contact with the binding sites, reducing attachment time.

Our previous studies have characterized acoustic streaming-induced removal of nonspecific binding of proteins in immunoassays. In finite element fluid solid interaction (FE-FSI) model simulations, we have established the mechanism for the removal of nonspecifically bound (NSB) proteins using Rayleigh SAWs.[22,23] We found that acoustic streaming can weaken effective interactions between targeted proteins, and facilitate removal of these undesired proteins. The three-dimensional coupled field FE-FSI model of a SAW device yielded insights into the NSB removal mechanism. The results indicated that SAWs induced a drag force arising from the tangential component of fluid velocity, which leads to particle advection, which is a key factor in removing biofouling. Effective removal of NSB proteins using a lithium niobate substrate based SAW device was experimentally demonstrated in our previous work as well.[24] The sensor signal is expected to be increased by this SAW-induced acoustic streaming, improving true determinations. In this work, we show that IF assays can be improved significantly by combining MEF with acoustic streaming from a SAW device. A lowered limit of detection in the clinically relevant range is achieved for the cancer marker CEA in a much shorter time than without MEF and acoustic streaming.

THEORY AND SIMULATION

Theoretical Analysis. Kümmerlen et al.[25] have developed a model to calculate the quantum yield enhancement factor Y (the ratio of the fluorescence intensity of the dye near the metal particle to that without a particle) described by the following equation:

$$Y = |L(\omega_{exc})|^2 Z(\omega_{flu}) \quad (1)$$

Here, the $|L(\omega_{exc})|^2$ term denotes the enhancement of local electric field at the excitation frequency ω_{exc} and the $Z(\omega_{flu})$ term represents the amplitude of quantum yield by radiation yield changes at the fluorescent frequency ω_{flu}. To evaluate the two terms in eq 1, the integrated near-field scattering cross section divided by the surface area of the particle was introduced by Messinger et al.[26] The near-field scattering cross section is given by

$$Q_{nf} = \frac{P_s}{P_i} = \frac{R^2}{\pi a^2}\int_0^{2\pi}\int_0^{\pi} \vec{E_S}\cdot\vec{E_S}^{*}\sin\theta\cdot d\theta d\phi|_{R=a} \quad (2)$$

where P_s and P_i are the scattered and incident power, respectively, for a given geometric cross section. R is the distance from the center of the metal nanoparticle and a is the radius of the particle. E_s represents the scattered electric field at the distance R. Q_{nf} can be a good measure of relative near-field intensification as a function of sphere size and incident wavelength. Messinger et al. have evaluated the near-field intensification for Ag, Cu, and Au spheres using Q_{nf}.[26] However, this theory and equations were established for spherical nanoparticles. Applying this theory to silver nanocubes would lead to inaccuracies.

The above model is applicable to estimate enhancement from a single sphere. It would appear that the real density of the silver cubes in the sensing area will affect the enhancement factor, which we have varied in this work to achieve optimal enhancement. Nakamura et al.[27] have considered the effect of particle density. They assumed that the number of fluorophores on the particle is the same as on the substrate in an area equivalent to the particle cross section. The total fluorescence intensity comes from two contributions: from the fluorophores on the particles and from the fluorophores on the substrate. The total intensity I_{tot} per unit area is given by

$$I_{tot} = S\delta I_{flu} + (1 - S)\delta I^0_{flu} \quad (3)$$

where S ($S = Nd^2$, N is the number of particles and d is the side length of the cube) and δ are the total cross section of particles and the number density of the fluorophores per unit area, respectively. I_{flu} and I^0_{flu} represents the intensity of the fluorophores on a particle and on the substrate, respectively. The derivative of total fluorescence intensity with respect to total cross section of particles is

DOI: 10.1021/acssensors.7b00876
ACS Sens. 2018, 3, 222−229

$$\frac{dI_{tot}}{dS} = \delta(I_{flu} - I^0_{flu}) \quad (4)$$

which suggests that, provided I_{flu} is greater than I^0_{flu}, the total fluorescence intensity increases with the particle density. In our work, the enhancement factors were positive implying that the total fluorescence intensity would continue to increase with increase in particle density.

Finite Difference Time Domain (FDTD) Simulations. Silver cubes were utilized in this work because the sharp edges and corners of the cubes are expected to enhance fluorescence better than equivalent spheres, which lack such field-intensifying edges and corners. The Finite Difference Time Domain (FDTD) simulation method was applied to compare the quantum yield enhancement between a silver cube and a sphere at different distances from the surface of the particle, which is assumed to be on the sensor surface. In these simulations, the radius of the sphere was set at 25 nm and the edge length of the cube was set at 50 nm, the targeted size in our nanoparticle synthesis, for comparison purposes. The distance between the dipole source (location of the fluorophore) and the surface of particles was set at 15, 25, and 50 nm. In our experiments, literature reported dimensions of CEA of 20 × 8 nm (length × width)[28] were utilized. The CEA capture and detection antibodies in our work are IgG1 isotype raised in mouse using human colon adenocarcinoma. The general length of IgG is in the range of 12−15 nm.[29,30] Since the sandwich structure was used in our experiment, the average distance between nanoparticle and fluorophore is estimated to be about 40 nm due to the twist. The dielectric constant of the medium was taken to be 1.00059 at room temperature, as our measurements were made in air. The wavelength of the source was varied in the range of 450 to 700 nm.

EXPERIMENTAL SECTION

Reagents and Apparatus. The materials and reagents utilized in our experiments and their sources are CEA capture antibody (Fitzgerald, 10-C10D), CEA detection antibody labeled with Alexa-488 (Fitzgerald, 10-C10E) (tagged with Alexa Fluor 488 Protein Labeling Kit, Thermo Fisher), CEA antigen (Abcam, ab742), PBS (Life Technologies, pH 7.4), and bovine serum albumin (BSA, Fisher Scientific). The materials used to synthesize the AgNCs included silver trifluoroacetate (CF_3COOAg, Sigma-Aldrich), HCl (37% in weight, Sigma-Aldrich), ethylene glycol (Sigma-Aldrich), NaSH (Sigma-Aldrich), and poly(vinylpyrrolidone) (PVP, Alfa Aesar). Reagent grade deionized water (DI water) with 18.2 MΩ-cm resistivity was produced in the laboratory using a Millipore system.

The instruments utilized in the experiments were Hitachi S-800 Scanning Electron Microscope; Leica DMI4000 B fluorescence microscope; Harrick Plasma, PDC-32G; and Rohde & Schwarz SMA100A signal generator.

Preparation of Silver Nanocubes. Silver nanocubes were synthesized using the method developed by Zhang et al.[31] This method utilizes ethylene glycol as the solvent and CF3COOAg as the precursor in a nucleation and growth solution process. It was adapted to synthesize AgNCs with a targeted edge length of about 50 nm. Two criteria were utilized in choosing this target size of AgNCs for synthesis: to maximize overlap of the surface plasmon resonance peak of the cubes with the excitation peak of the fluorophore, and ease of synthesis. Cubes of edge length near about 75 nm are indicated for best overlap with the excitation peak of Alexa 488; however, letting the growth part of the nucleation and growth mechanism proceed longer to allow sizes larger than 50 nm results in loss of shape of the synthesized particles. Most of our synthesis yielded particles in the range of 40 to 50 nm. An SEM image and the UV−vis absorption spectra for one of the synthesis of these AgNCs are shown in Figure 1. The two distinctive shoulders to the left of the main peak in the UV−vis spectrum, visible for all of our synthesized samples, is indicative of cubes being formed. Analysis using TEM images (60−70 samples) was utilized to determine size and percentage of cubes formed. In most synthesis attempts, about 70−80% of particles were found to be cubes; however, monodisperse AgNCs were not realized in our synthesis attempts. Colloidal synthesis of monodisperse AgNCs is difficult, especially when scaled up to produce sufficient quantities necessary for our experiments. These AgNCs were stored in DI water.

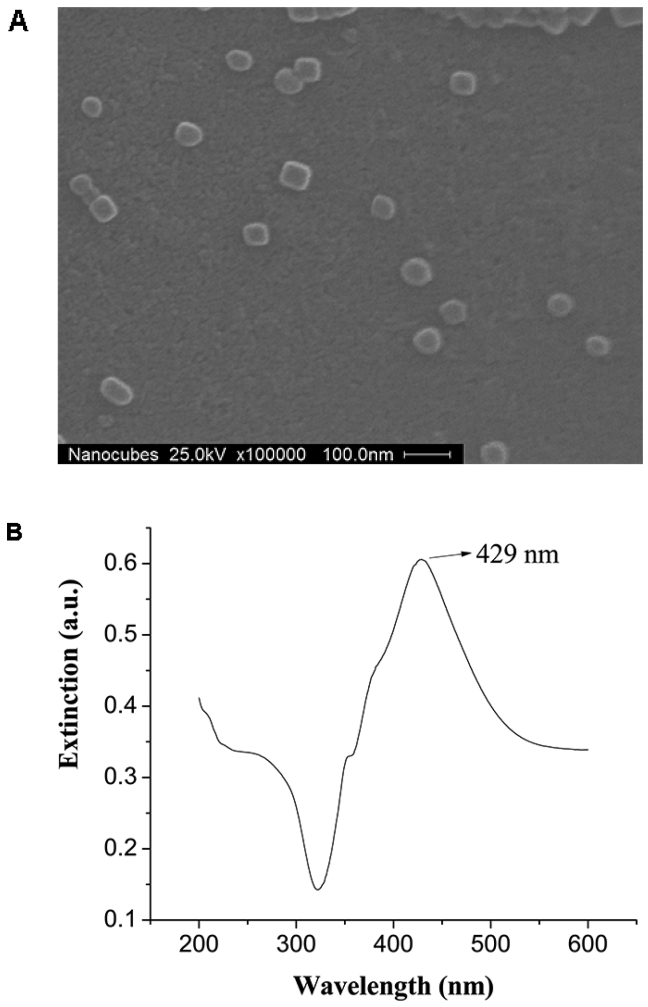

Figure 1. SEM image and extinction spectrum of the synthesized silver nanocubes. Particles were dispersed in DI water for the UV−vis measurement.

Antigen Immobilization and Detection with MEF. Two groups of glass slides were set up and cleaned using a piranha solution (4 parts of concentrated sulfuric acid and 1 part of 30% hydrogen peroxide solution). A solution of (3-aminopropyl)-triethoxysilane (3-APTES, Sigma-Aldrich) in pure ethanol (1% in volume) was prepared to pretreat the surface of the slides for immobilization of the AgNCs and the capture antibodies. After drying with nitrogen, both groups of slides were treated with the 3-APTES solution on the surface and 30 μL of AgNCs solution was immobilized on the surface of one group of slides overnight. 30 μL of 10 μg/mL CEA capture antibody were added to the surface of the glass sides in both groups followed by incubation for 1 h at room temperature. The slides were thoroughly rinsed with PBS three times. PBS rinsing followed every incubation procedure in all experiments. 1% of BSA in PBS solution was used to block the extra binding sites of 3-APTES and on the surface by adding 30 μL of BSA and incubating for 1 h. CEA

DOI: 10.1021/acssensors.7b00876
ACS Sens. 2018, 3, 222−229

was diluted to the desired concentrations of 1 ng/mL, 10 ng/mL, 100 ng/mL, 1 μg/mL, and 10 μg/mL with PBS solution. After rinsing, 20 μL of different concentrations of CEA antigen from 1 ng/mL to 10 μg/mL were added and incubated for 45 min. Following this, 10 μL of CEA detection antibody, labeled with Alexa-488, at an approximate concentration of 10 μg/mL was added and incubated for another 45 min. A Leica DMI4000 B microscope was utilized for fluorescence measurements. The concentrations of CEA capture antibody and CEA detection antibody labeled with dye were held constant in all experiments. The experiment was repeated three times for each concentration of CEA antigen. Figure 2 illustrates the MEF experiments schematically.

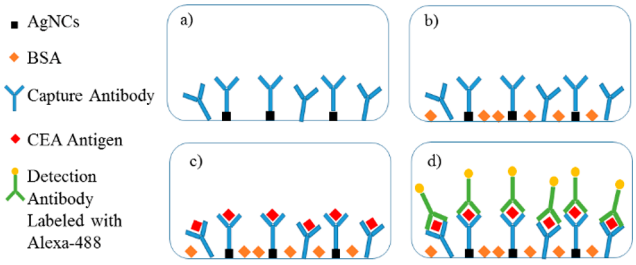

Figure 2. Schematic diagram of the MEF experiment. (a) Ag nanocubes were immobilized on the surface of the glass slides via APTES and CEA capture antibody was incubated above them; (b) BSA was added to block the excess binding sites; (c) CEA antigen was then added and bound to the capture antibody; (d) CEA detection antibody labeled with Alexa-488 was added and bound to the CEA antigen.

Dependence of MEF on AgNC Area Density. To investigate the dependence of MEF on AgNC area density, a set of 5 glass slides were attached (using 3-APTES as before) with different concentrations of AgNCs in DI water to achieve increasing areal densities. MEF was measured using the previously described procedure. 10 μL of CEA in PBS at an approximate concentration of 10 μg/mL was utilized for these measurements. MEF was quantified with the microscope as described before. The slides differed only in the area density of AgNCs (one was a control with no nanocubes) with all the other conditions kept the same.

Mixing and NSB Protein Removal Using Acoustic Streaming. The effects of increased mixing between antigen and antibody and the removal of NSB proteins due to acoustic streaming generated by Rayleigh SAWs was quantified using fluorescence measurements. Rayleigh SAWs were generated using delay-line SAW devices fabricated in 128° rotated Y-cut X-propagation lithium niobate ($LiNbO_3$) substrates, which were utilized to replace the glass slides as the experimental platform. The devices were fabricated using standard photolithography. Au/Cr interdigital transducers having 60 pairs of electrodes were patterned on the substrate with finger width of 10 μm and a delay path of 8000 μm. The fabricated devices had a center frequency of approximately 79 MHz.

Two types of experiments were conducted. The first was designed to quantify the mixing effect by comparing a series of chips treated differently. Four $LiNbO_3$ chips were first cleaned by acetone, methanol, and DI water rinsing, after which they were dried with nitrogen. A PDMS cell was bound to the device surface via electric charge interaction. The device surfaces were silanized and AgNCs were applied to all the chips. Initially, 30 μL of 100 μg/mL of CEA capture antibody was added to the surface and incubated for 1 h. Then, BSA was applied to block the excess binding sites. At this point, 20 μL of 10 μg/mL of CEA antigen was added to all of the chips and incubated for another 1 h. Then, 20 μL of detection antibody labeled with fluorophores of approximately 10 μg/mL concentration was added, and each chip was incubated under different conditions. Two chips were incubated without acoustic streaming for 10 and 60 min, respectively. The other two were incubated with the SAW device operated at 0 dBm (equal to 1 mW) of streaming power for 5 and 10 min, respectively. The chips were then rinsed with PBS solution and fluorescence intensity was quantified with the Leica fluorescence microscope.

The second experiment was designed to demonstrate NSB protein removal with acoustic streaming. The chips were cleaned and dried, and then the PDMS cells were bound to the surface. After silanization, AgNCs were attached, after which 30 μL of 1% BSA was added to the surface and incubated for 1 h. After rinsing with PBS, 20 μL of fluorophore-labeled detection antibody of about 10 μg/mL concentration was added and incubated for another hour. After completely washing with PBS, fluorescence intensity was quantified using the microscope. Next, the chip was set up with the signal generator to apply the surface acoustic waves for the removal. 10 μL of PBS was added before turning on the power. The initial power was set at 0 dbm and lasted for 10 min. The second step also consisted of applying 10 min of power at 0 dbm. The third and last removal step consisted of applying 3 dbm of power (2 mW) for 10 min. Fluorescence intensity was quantified after each of these three removal steps. Figure 3 shows the schematic diagram of the NSB protein removal process with the devices.

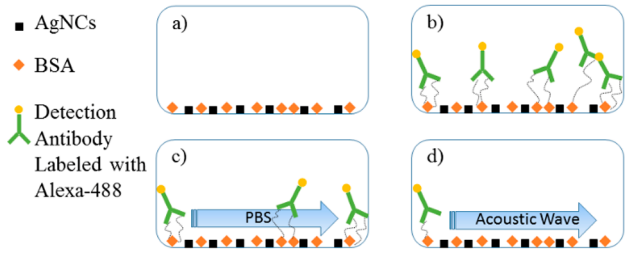

Figure 3. Schematic diagram of NSB protein removal process with SAWs. (a) Ag nanocubes were immobilized on the surface of the chip via APTES and BSA was used to block the surface. (b) CEA detection antibody labeled with Alexa-488 was added and nonspecifically bound. (c) Rinsed with PBS three times. (d) Removal was done with SAWs.

RESULTS AND DISCUSSION

Simulation Results. The simulated quantum yield enhancement as a function of wavelength in the range of 450−700 nm is plotted in Figure 4 for the sphere and the cube for the 3 distances considered. The cube leads to a larger quantum yield enhancement than the sphere at long wavelengths, especially when the wavelength is longer than 450 nm.

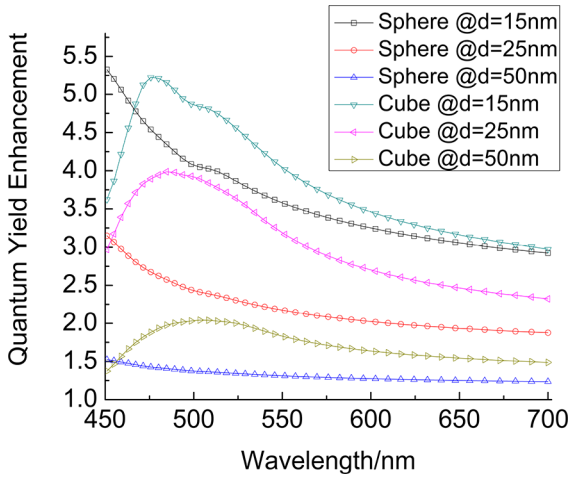

Figure 4. Simulated quantum yield enhancement results for a sphere and a cube at different distances from the particle surface.

DOI: 10.1021/acssensors.7b00876
ACS Sens. 2018, 3, 222−229

Most fluorophores emit at longer wavelengths, as does the Alexa 488 fluorophore used in our experiment, which emits at 519 nm. Therefore, the results at this wavelength are presented in Figure 5 below. These simulations indicate that the cube is

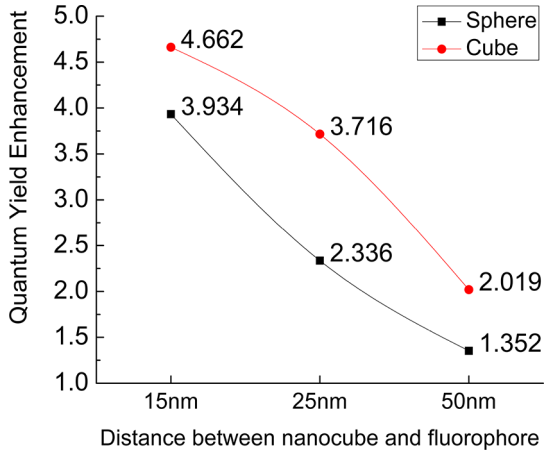

Figure 5. Quantum yield enhancement for a sphere and a cube at 519 nm, the emission wavelength for Alexa 488.

more effective in enhancing the fluorescence intensity, including at the estimated nanoparticle−fluorophore distance of about 40 nm in our experiments. Another conclusion from the figure is that within the effective range, the enhancement decreases as the distance from the fluorophore to the particle surface increases. Hence, the precise control of the distance between the particle and the fluorophore is an essential factor for this fluorescence enhancement technique.

MEF Results. Fluorescence images of each slide were taken by the Leica microscope and the pixel intensity was determined and color coded with the software ImageJ. Figure 6 summarizes the MEF results.

Five concentrations of CEA antigen were detected with and without AgNCs to quantify MEF. Triplicate measurements were made, which exhibited small standard deviations. The intensity enhancement factors for different concentrations varied in the range of 3.9 to 5.4. It is apparent from these results that AgNCs enhance signal intensity sufficiently to lower the detection limit to below 1 ng/mL. Fluorescence intensity is linear in log (conc) (ng/mL) over the range of 1−1000 ng/mL, as shown in Figure 6C. Sensitivity of the sensor with AgNCs is calculated to be about 6 times larger than that without, due to MEF. The signal at 100 pg/mL is measurable and larger than the measurement error. Hence, this device exhibits a limit of detection lower than 1 ng/mL. Without MEF, a concentration of over 100 ng/mL is required to achieve similar intensities as with 1 ng/mL and MEF, indicating 2−3 orders of magnitude reduction of the LOD with MEF. These results are encouraging and clearly indicate that an optimized device with MEF could lower the LOD to less than 100 pg/mL of CEA in the solution.

Optimization of Area Density of AgNCs. Area density of the AgNCs, among other factors, affects MEF, via controlling distance between the nanocubes and fluorophores. Thus, the density of AgNCs distributed on the chip was varied to study this effect.

Five different area densities were studied. SEM images and pseudo color MEF photographs at these area densities are shown in Figure 7. Enhancement increases with area density up to a point, after which it decreases. In this case, an

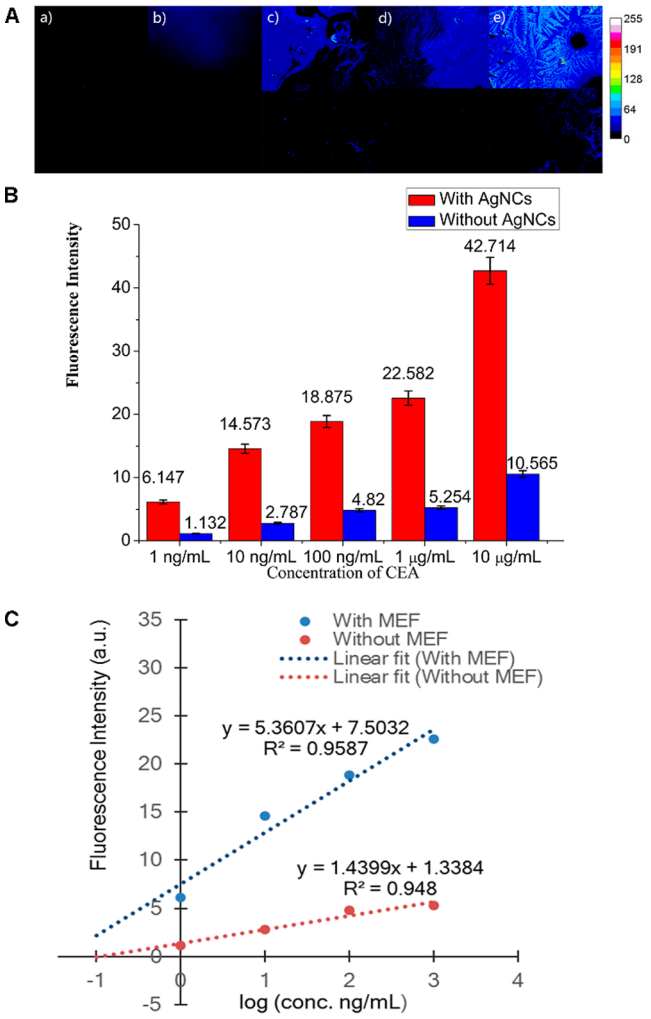

Figure 6. Results of the MEF experiment using AgNC area density of 37.2−46.5 cubes/μm^2 from SEM image analysis. (A) Top row of the fluorescence images are for the group with AgNCs of approximately 50 nm edge length. The bottom row is for the corresponding controls, i.e., with no AgNCs. The concentration of CEA antigen used was (a) 1 ng/mL, (b) 10 ng/mL, (c) 100 ng/mL, (d) 1 μg/mL, and (e) 10 μg/mL. (B) Fluorescence intensities. (C) Linear fits of intensity vs log (conc.) (ng/mL) in the range of 1−1000 ng/mL.

enhancement factor of between 6 and 7 is realized for the area density of about 80 cubes/μm^2. It is expected that the fluorescence signal intensity would drop at high nanocube densities for two reasons: One is that AgNCs occupy too many binding sites on the surface interfering with antigen/antibody incubation on the chip. Another is that the high particle density blocks the light path. The optimized enhancement factor of about 7 relative to an assay without AgNCs is reasonably large to construct a useful sensor. Further increase in enhancement factor can be achieved by optimizing other variables that affect MEF, in particular, nanocube−fluorophore distance and overlap of the LSPR absorption peak with excitation wavelength. The results of this study indicate that the edge length of the AgNCs should be larger than 50 nm to achieve better overlap at the fluorophore absorption wavelength of 488 nm. However, with the colloidal synthesis route employed in this work, it is difficult to retain cubic shape if the growth part of the cube formation process is allowed to continue toward much larger particle size than 50 nm.

DOI: 10.1021/acssensors.7b00876
ACS Sens. 2018, 3, 222−229

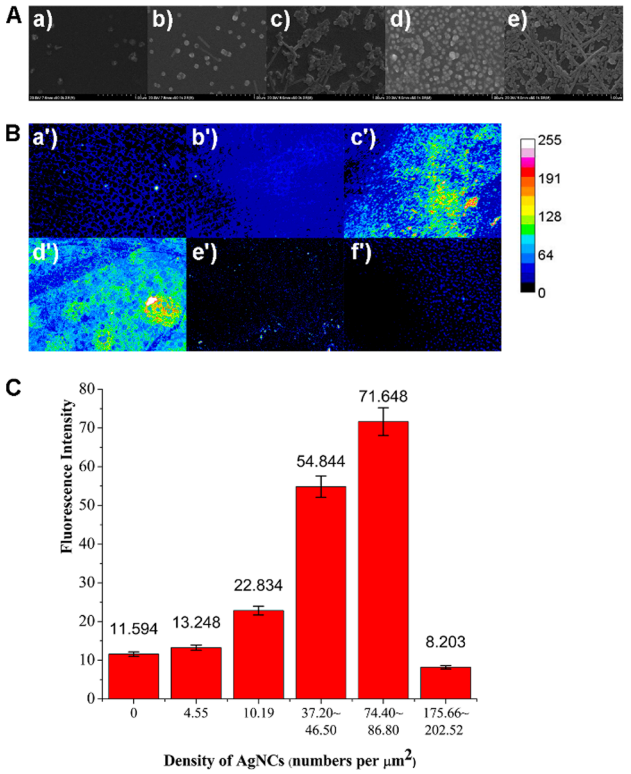

Figure 7. Different area densities of the AgNCs distributed on the chips visualized with SEM (image analyzed at 3 locations on the surface) are (a) 4.5, (b) 10.2, (c) 37.2−46.5, (d) 74.4−86.8, and (e) 175.7−202.5 cubes/μm^2 and the corresponding MEF signal intensities are shown in the photographs (b′) to (f′) while (a′) is the intensity without AgNCs on the chip.

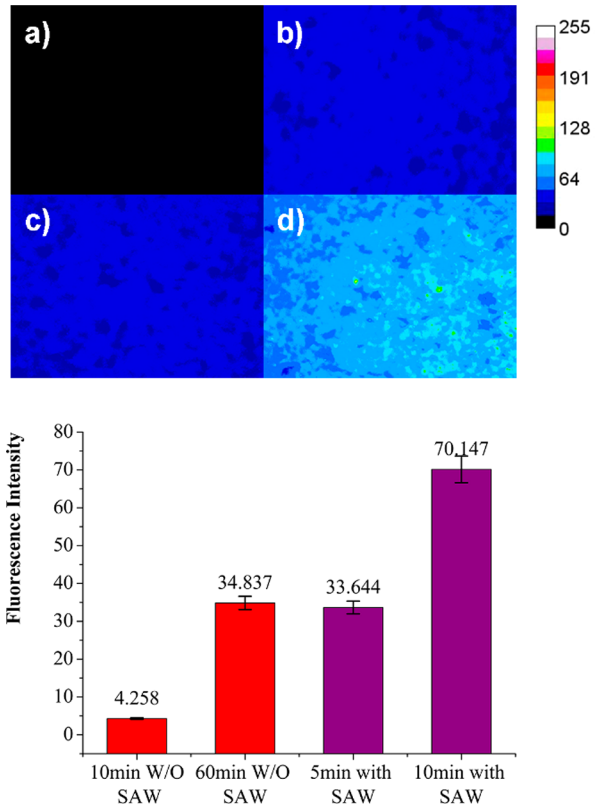

Figure 8. Enhancing the mixing effect with SAWs. Chip (a) was treated without SAW for 10 min; (b) was treated without SAW for 60 min; (c) was treated with SAW for 5 min at 0 dBm; (d) was treated with SAW for 10 min at 0 dBm.

Increased Mixing and Nonspecific Binding Removal Using Acoustic Streaming by Rayleigh SAWs. Acoustic streaming induced by Rayleigh SAWs was utilized to address other issues associated with low working efficiency of this IF assay.

Incubation time was shortened from several hours to several minutes and binding percentage was simultaneously increased upon streaming. Removal of NSB proteins was also studied quantitatively. These improvements to the IF assay from acoustic streaming have the potential to decrease background noise, ultimately resulting in reduced false positives. Fluorescence images from the mixing studies using the SAW device are presented in Figure 8. From the results presented in the 4 images, reduction in incubation time is clearly evident. Upon application of acoustic streaming, signal strength reached the same level with 5 min of streaming as that of 60 min without. An additional 5 min of streaming increased the fluorescence signal to over twice the value, which did not change any further with further exposure to acoustic waves.

In general, SAW-based acoustic streaming is able to accelerate the mixing between antigen and antibody by a factor of 12 and helps overcome the diffusion limitation by increasing the signal by a factor of 2. Results for SAW-based NSB removal are shown in Figure 9. Four fluorescence images at different stages were taken as follows: (a) after the PBS rinse, (b) after 10 min of removal with the SAW at 0 dBm, (c) after an additional 10 min of removal at 0 dBm, and (d) a third 10 min removal at 3 dBm.

It is clear, from both the fluorescence images and the quantification of intensity, that NSB-proteins between CEA detection antibody and BSA or the AgNCs are efficiently and effectively removed using SAW-based streaming. What is not possible with extensive chemical rinsing is easily removed by SAW forces in a reasonable time frame. These results indicate that IF assays done on a SAW device have great potential to minimize the effect of background noise. SAW devices reduced background signal by a factor of 6 in this work by removing NSB proteins.

■ CONCLUSIONS AND PROSPECTS

To summarize, this work focused on the combination of metal-enhanced fluorescence and surface acoustic wave devices to detect the CEA antigen at clinically significant levels with immunofluorescence assays. The limit of detection of CEA antigen was successfully brought from 1 μg/mL down to subnanogram/mL levels. Incubation times were reduced tremendously by acoustic streaming with Rayleigh SAWs. NSB proteins, which interfere with the fluorescence signal, were shown to be removed much more effectively than with chemical rinsing alone, again using SAW-based acoustic streaming. These improvements are brought about by the introduction of a substrate based on a SAW device with bound silver nanocubes on the surface for the IF assay. The dependence of enhancement on the area density of silver nanocubes was studied, which allows for further optimization of the sensor. Overall, this study enables construction of sensor substrates and IF assays for sensitive detection and quantification of cancer

DOI: 10.1021/acssensors.7b00876
ACS Sens. 2018, 3, 222−229

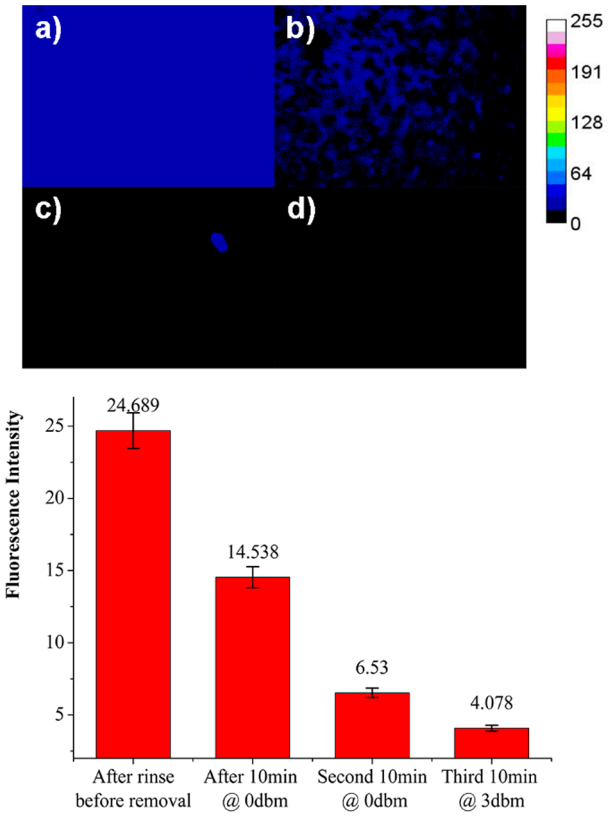

Figure 9. Fluorescence intensities of nonspecific binding removal with SAWs: (a) after the rinse, but before the removal; (b) after 10 min of removal process at 0 dBm; (c) after the second 10 min of removal process at 0 dBm; and (d) after the third 10 min of removal process at 3 dBm.

biomarkers in clinically relevant subnanogram/mL levels in body fluids such as blood and urine.

AUTHOR INFORMATION

Corresponding Author

*E-mail: bhethana@usf.edu.

ORCID

Venkat R. Bhethanabotla: 0000-0002-8279-0100

Author Contributions

All authors have given approval to the final version of the manuscript.

Notes

The authors declare the following competing financial interest(s): A patent has been filed on results related to this research.

ACKNOWLEDGMENTS

This work was funded by the National Science Foundation grant number IIP-1640668, which is gratefully acknowledged.

REFERENCES

(1) IARC *World Cancer Report 2014*; 2014.

(2) Gold, P.; Freedman, S. O. Specific carcinoembryonic antigens of the human digestive system. *J. Exp. Med.* **1965**, *122* (3), 467−481.

(3) Ballesta, A.; Molina, R.; Filella, X.; Jo, J.; Gimenez, N. Carcinoembryonic antigen in staging and follow-up of patients with solid tumors. *Tumor Biol.* **1995**, *16* (1), 32−41.

(4) Duffy, M. J. Carcinoembryonic Antigen as a Marker for Colorectal Cancer: Is It Clinically Useful? *Clinical Chemistry* **2001**, *47* (4), 624−630.

(5) Thomson, D.; Krupey, J.; Freedman, S.; Gold, P. The radioimmunoassay of circulating carcinoembryonic antigen of the human digestive system. *Proc. Natl. Acad. Sci. U. S. A.* **1969**, *64* (1), 161−167.

(6) Goldsby, R. A.; Kindt, T. J.; Osborne, B. A.; Kuby, J. *Immunology*; WH Freeman: New York, 2003.

(7) Pompa, P. P.; Martiradonna, L.; Torre, A. D.; Sala, F. D.; Manna, L.; De Vittorio, M.; Calabi, F.; Cingolani, R.; Rinaldi, R. Metal-enhanced fluorescence of colloidal nanocrystals with nanoscale control. *Nat. Nanotechnol.* **2006**, *1* (2), 126−30.

(8) Aslan, K.; Lakowicz, J. R.; Geddes, C. D. Metal-enhanced fluorescence using anisotropic silver nanostructures: critical progress to date. *Anal. Bioanal. Chem.* **2005**, *382* (4), 926−933.

(9) Aslan, K.; Leonenko, Z.; Lakowicz, J. R.; Geddes, C. D. Annealed silver-island films for applications in metal-enhanced fluorescence: interpretation in terms of radiating plasmons. *J. Fluoresc.* **2005**, *15* (5), 643−54.

(10) Aslan, K.; Malyn, S. N.; Geddes, C. D. Metal-enhanced fluorescence from gold surfaces: angular dependent emission. *J. Fluoresc.* **2006**, *17* (1), 7−13.

(11) Malicka, J.; Gryczynski, I.; Gryczynski, Z.; Lakowicz, J. R. Effects of fluorophore-to-silver distance on the emission of cyanine-dye-labeled oligonucleotides. *Anal. Biochem.* **2003**, *315* (1), 57−66.

(12) Chowdhury, S.; Bhethanabotla, V. R.; Sen, R. Silver-copper alloy nanoparticles for metal enhanced luminescence. *Appl. Phys. Lett.* **2009**, *95* (13), 131115.

(13) Aslan, K.; Gryczynski, I.; Malicka, J.; Matveeva, E.; Lakowicz, J. R.; Geddes, C. D. Metal-enhanced fluorescence: an emerging tool in biotechnology. *Curr. Opin. Biotechnol.* **2005**, *16* (1), 55−62.

(14) Aslan, K.; Lakowicz, J. R.; Szmacinski, H.; Geddes, C. D. Metal-enhanced fluorescence solution-based sensing platform. *J. Fluoresc.* **2004**, *14* (6), 677−679.

(15) Morton, S. M.; Silverstein, D. W.; Jensen, L. Theoretical studies of plasmonics using electronic structure methods. *Chem. Rev.* **2011**, *111* (6), 3962−3994.

(16) Chowdhury, S.; Bhethanabotla, V. R.; Sen, R. Effect of Ag− Cu alloy nanoparticle composition on luminescence enhancement/quenching. *J. Phys. Chem. C* **2009**, *113* (30), 13016−13022.

(17) Huber, K.; Kirchheimer, J. C.; Sedlmayer, A.; Bell, C.; Ermler, D.; Binder, B. R. Clinical value of determination of urokinase-type plasminogen activator antigen in plasma for detection of colorectal cancer: comparison with circulating tumor-associated antigens CA 19−9 and carcinoembryonic antigen. *Cancer Res.* **1993**, *53* (8), 1788−1793.

(18) Tang, H.; Chen, J.; Nie, L.; Kuang, Y.; Yao, S. A label-free electrochemical immunoassay for carcinoembryonic antigen (CEA) based on gold nanoparticles (AuNPs) and nonconductive polymer film. *Biosens. Bioelectron.* **2007**, *22* (6), 1061−1067.

(19) Chon, H.; Lee, S.; Yoon, S.-Y.; Chang, S.-I.; Lim, D. W.; Choo, J. Simultaneous immunoassay for the detection of two lung cancer markers using functionalized SERS nanoprobes. *Chem. Commun.* **2011**, *47* (46), 12515−12517.

(20) Paxton, W. F.; O'Hara, M. J.; Peper, S. M.; Petersen, S. L.; Grate, J. W. Accelerated analyte uptake on single beads in microliter-scale batch separations using acoustic streaming: plutonium uptake by anion exchange for analysis by mass spectrometry. *Anal. Chem.* **2008**, *80* (11), 4070−4077.

(21) Toegl, A.; Kirchner, R.; Gauer, C.; Wixforth, A. Enhancing results of microarray hybridizations through microagitation. *J. Biomol. Tech* **2003**, *14* (3), 197−204.

(22) Sankaranarayanan, S. K.; Cular, S.; Bhethanabotla, V. R.; Joseph, B. Flow induced by acoustic streaming on surface-acoustic-wave devices and its application in biofouling removal: A computational study and comparisons to experiment. *Phys. Rev. E* **2008**, *77* (6), 066308.

DOI: 10.1021/acssensors.7b00876
ACS Sens. 2018, 3, 222−229

(23) Singh, R.; Sankaranarayanan, S. K.; Bhethanabotla, V. R. Enhanced surface acoustic wave biosensor performance via delay path modifications in mutually interacting multidirectional transducer configuration: A computational study. *Appl. Phys. Lett.* **2009**, *95* (3), 034101.
(24) Cular, S.; Branch, D. W.; Bhethanabotla, V. R.; Meyer, G. D.; Craighead, H. G. Removal of nonspecifically bound proteins on microarrays using surface acoustic waves. *IEEE Sens. J.* **2008**, *8* (3), 314−320.
(25) Kümmerlen, J.; Leitner, A.; Brunner, H.; Aussenegg, F.; Wokaun, A. Enhanced dye fluorescence over silver island films: analysis of the distance dependence. *Mol. Phys.* **1993**, *80* (5), 1031−1046.
(26) Messinger, B. J.; Von Raben, K. U.; Chang, R. K.; Barber, P. W. Local fields at the surface of noble-metal microspheres. *Phys. Rev. B: Condens. Matter Mater. Phys.* **1981**, *24* (2), 649.
(27) Nakamura, T.; Hayashi, S. Enhancement of dye fluorescence by gold nanoparticles: analysis of particle size dependence. *Jpn. J. Appl. Phys.* **2005**, *44* (9R), 6833.
(28) Hammarström, S. The carcinoembryonic antigen (CEA) family: structures, suggested functions and expression in normal and malignant tissues; *Seminars in cancer biology*; Elsevier, 1999; pp 67−81.
(29) Silverton, E.; Navia, M. A.; Davies, D. R. Three-dimensional structure of an intact human immunoglobulin. *Proc. Natl. Acad. Sci. U. S. A.* **1977**, *74* (11), 5140−5144.
(30) Lee, J. F.; Stovall, G. M.; Ellington, A. D. Aptamer therapeutics advance. *Curr. Opin. Chem. Biol.* **2006**, *10* (3), 282−289.
(31) Zhang, Q.; Li, W.; Wen, L. P.; Chen, J.; Xia, Y. Facile synthesis of Ag nanocubes of 30 to 70 nm in edge length with CF3COOAg as a precursor. *Chem. - Eur. J.* **2010**, *16* (33), 10234−10239.

DOI: 10.1021/acssensors.7b00876
ACS Sens. 2018, 3, 222−229